Magnetic Composite for Efficient Adsorption of Iron and Manganese Ions from Aqueous Solution

Widia Purwaningrum[1,2], Hasanudin[2], Addy Rachmat[2],
Fahma Riyanti[1,2], Poedji Loekitowati Hariani[2*]

[1] Doctoral Program, Faculty Mathematics and Natural Sciences, Universitas Sriwijaya, Palembang 30139, South Sumatra, Indonesia

[2] Department of Chemistry, Faculty of Mathematics and Natural Sciences, Universitas Sriwijaya, Jalan Palembang-Prabumulih, Indralaya, Ogan Ilir 30862, Indonesia

* Corresponding author's email: puji_lukitowati@mipa.unsri.ac.id

ABSTRACT

Iron Fe(III) and Manganese Mn(II) ions were effectively removed from aqueous solutions using a magnetic composite of Fe_3O_4/CaO/PDA, with CaO sourced from green mussel. The composite material was comprehensively characterized using Fourier Transform Infrared Spectroscopy (FTIR), X-ray Diffraction (XRD), Scanning Electron Microscopy with Energy Dispersive – X-ray Spectroscopy (SEM-EDS), Brunauer, Emmett and Teller (BET) surface area analysis, Vibrating Sample Magnetometer (VSM). The impact of physicochemical adsorption parameters, such as solution pH, contact time, and concentration, were investigated. The Fe_3O_4/CaO/PDA composite displayed a value of 51.47 emu/g in saturation magnetization, enabling rapid separation through the use of an external magnet without the need for filtration. Optimal conditions for adsorbing Fe(III) ions were achieved at pH 3 and initial concentration of 400 mg/L with maximum efficiency reach after 60 minutes. Similarly, optimal conditions for Mn(II) ion adsorption were observed at pH 4 with the same contact time and initial concentration. The adsorption efficiencies were found to be 88.56% for Fe(III) and 75.65% for Mn(II). The pseudo-second-order model aptly depicted the kinetics associated with the adsorption of both types of ions while the Langmuir isotherm model indicated that monolayer adsorption takes place on the composite's surface. The maximum capacities for adsorption is 322.58 mg/g for Fe(III) ions and 208.33 mg/g for Mn(II) ions. A negative Gibbs free energy value affirmed that the process occurs spontaneously under natural conditions. These results underscored the potential use of this Fe_3O_4/CaO/PDA composite in treating wastewater to remove heavy metal ions.

Keywords: magnetic composite; adsorption; iron and manganese ions

INTRODUCTION

Currently, the environmental repercussions of mining are a significant global concern (Valente et al., 2015; Nunex-Gomez et al., 2019). The extraction and processing of coal result in the disposal of wastewater in open areas that are particularly rich in pyrite. The oxidation process occurs in the presence of water, oxygen, and microbes, forming Acid Mine Drainage (AMD) (Mokgehle and Tawengwa, 2021; Kobielska et al., 2018). In addition, it should be noted that AMD possesses the ability to dissolve heavy metal ions.

Consequently, the defining attributes of AMD include a low pH level, typically below 4.0, as well as elevated concentrations of sulfides and various heavy metal including but not limited to Fe, Al, Mn, Cu, Zn, Pb, Ni, Cd, and Co (Nunex-Gomez et al., 2019; Yang et al., 2021). AMD presents a considerable risk of contaminating both underground and surface water bodies, thereby creating substantial environmental issues that can negatively affect ecosystems and human health (Ren et al., 2022; Favere et al., 2004). Metal ions with high atomic weights pose challenges for natural decomposition processes, as they have a tendency

to infiltrate the food chain and accumulate within animals (Masindi et al., 2015).

The concentrations of heavy metals in AMD have been lowered using a variety of different approaches. These methods include sulfidogenic bioreactors (Deng et al., 2016), reverse osmosis (Ambiado et al., 2017), membrane filtration (Menzel et al., 2021), electrocoagulation using $Ca(OH)_2$ (Stylianou et al., 2022), microalgae phycoremediation (Chen et al., 2023), and adsorption using layered double hydroxides (Xu et al., 2023). There is an immediate need for AMD processing technologies that are not only effective but also affordable and capable of eliminating significant quantities of metal ions. There is reason to be optimistic about the adsorption approach to solving this issue.

CaO, a potential natural adsorbent for the removal of heavy metal ions, can be sourced from a diverse range of materials. For instance, cow bones (Ayodeji, 2018), eggshells (Hossain et al., 2021), cockle shells (Mohamed et al., 2016), fish bones (Mostofa et al., 2022), and mollusk shells (Thakur et al., 2021) have all been identified as viable sources. Additionally, mussel shells – a type of shellfish widely consumed in Indonesia – are also an abundant source of CaO (Purwaningrum et al., 2022). Approximately 20% of the shellfish constitute the edible portion, while the remaining 75–90% comprises the shell. The composition of the mussel shell is mainly consisting of approximately 95% CaO, with the remaining constituents comprising organic matter and various other components (Aguila-Almanza et al., 2022; Hamestera et al., 2012). Hence, it is imperative to undertake the processing of mussel shell in order to mitigate environmental pollution.

The production of CaO can be achieved by subjecting $CaCO_3$ to elevated temperatures (Hossain et al., 2023). The utilization of natural adsorbents has been found to result in reduced operational expenses and exhibit environmentally sustainable characteristics. It is essential to acknowledge that natural adsorbents possess certain limitations, most notably their relatively low adsorption capacity. Hence, it is imperative to devise a novel adsorbent that can effectively address these constraints, primarily by modifying the adsorbent material. The formation of Fe_3O_4/CaO/PDA composite can be achieved by modifying CaO with Fe_3O_4 and polydopamine (PDA) compounds. Incorporating a superparamagnetic core, like Fe_3O_4, during the post-adsorption phase significantly improves efficiency. It allows for quick

adsorbent separation from the solution using a permanent magnet. This method is more economical than traditional filtration and centrifugation techniques (Hariani et al., 2021).

PDA is recognized for its biocompatibility and its unique ability to form a consistent layer that is hydrophilic in nature. This layer, characterized by functional groups on its surface, originates from the self-polymerization process of dopamine under alkaline buffer conditions. With superior adhesive characteristics and beneficial reducibility, PDA plays a crucial role in preventing Fe_3O_4/CaO from clustering (Yang et al., 2019). The versatility of PDA as an adsorbent has been showcased in various studies. For example, Fe_3O_4/PDA/PANI has been utilized as an adsorbent for eliminating tartrazine and Sunset yellow (Miri et al., 2021), MnO_2/PDA/Fe_3O_4 demonstrated potential for Pb(II) ions adsorption (Shi et al., 2021), and AMP/PDA/Fe_3O_4 proved effective for Cs(I) and U(VI) adsorption (Li et al., 2023).

This research aims to fabricate a Fe_3O_4/CaO/PDA composite using CaO sourced from green mussel shells. The characterization of this composite will involve methods such as FTIR, SEM-EDS, BET surface area analysis, XRD, and VSM. The main application of the synthesized composite will be for the adsorption of heavy metal, with a particular focus on Fe(III) and Mn(II) ions.

MATERIALS AND METHODS

Materials

The current investigation utilized a range of chemicals including but not limited to Iron(III) chloride hexahydrate, ethanol, Iron(II) chloride tetrahydrate, hydrochloric acid and sodium hydroxide. Additionally, Tris-Hydrochloride (Tris-Cl), Dopamine (DA), and standard solutions of Iron(II), Iron(III), and manganese(II) each with a concentration of 1000 ppm were used. All these chemicals were procured from Merck in Germany. Green mussel shells also played a part in the research process.

CaO preparation

The production of CaO in this study adheres to the method detailed by Purwaningrum et al. (2022). The process begins with the cleaning of green mussel shells to rid them of impurities. This is achieved by first rinsing the shells with distilled

water and subsequently boiling them for half an hour. Post-cleaning, the shells are oven-dried at a temperature of 100°C for a duration of two hours. Following this, the material is subjected to ball milling to obtain finer particles. The milled product is then calcinated in a muffle furnace at 800°C for an hour, with the temperature increasing at a steady rate of 3.5°C per minute. Finally, CaO is preserved in separate air-tight polyethylene bags to maintain its quality and prevent exposure to air.

The synthesis of Fe_3O_4/CaO/PDA composite

The synthesis of the Fe_3O_4/CaO/PDA composite was a two-step process. Initially, a Fe_3O_4/CaO composite was synthesized, adhering to a Fe_3O_4 to CaO mass ratio of 1:2. In total, 4.66 g of $FeCl_2 \cdot 6H_2O$ and 1.72 g of $FeCl_2 \cdot 4H_2O$ were collectively dissolved into a volume of 25 mL distilled water. This solution was mechanically stirred, while being continuously purged with nitrogen gas and heated to 60°C, followed by the gradual addition of 4 g CaO. Thereafter, a 1 M NaOH solution was introduced gradually until the solution reached a pH of 10. The resulting solid substance underwent washing with distilled water and ethanol until it attained neutral pH, after which it was dried in an oven at a temperature setting of 80°C for one hour. The second stage of the synthesis involved combining 2.0 g of CaO/FeO, 0.133 g of DA, and 0.22 g of Tris-Cl in a fresh volume (30 mL) of distilled water to create the final Fe_3O_4/CaO/PDA composite. The solution was then sonicated for two hours at room temperature, after which any suspended particles were separated via centrifugation at a speed of 3500 rpm for 30 minutes. The product was repeatedly washed with distilled water until it reached a netral pH level. The solid material was then extracted from the solution using an external magnet and subsequently dried in an oven set at 105°C for two hours.

CHARACTERIZATION

The analysis of the phase and crystal structure was executed using XRD (XRD PANalytical), with the settings being a 50-mA current, a 40 kV voltage, and CuKα radiation of 1.546 Å wavelength. BET technique was used to assess the surface area and pore size distribution of the adsorbent, involving nitrogen adsorption-desorption cycles on a QuadraSorb station 1 7.01. The morphology and elemental composition were examined using SEM-EDS (JOEL JSM 6510 LA). The magnetic characteristics of the adsorbent were probed using a VSM of Oxford Type 1.2 T model. FTIR conducted on a Prestige-21 Shimadzu instrument in the spectral range between 400–4000 cm^{-1}, was used for functional group analysis. Lastly, AAS on a Shimadzu AA 7000 was used to determine metal ion concentrations.

Adsorption

The adsorption capacity of the Fe_3O_4/CaO/PDA composite for Fe(III) and Mn(II) ions was assessed in this study. Various parameters were considered, including pH, contact time, initial concentration of metal ions in the solution, and temperature. The pH levels were adjusted to fall within a range of 1.5 to 5 using either a 1 M HCl or NaOH solution. The contact duration was varied between 0 and 70 minutes, while the initial concentration of ions in the solution was set within a range from 100 to 450 mg/L. Adsorption kinetics were examined by observing changes over varying contact times, while adsorption isotherms were derived from studying variations in the initial concentrations of metal ions. Thermodynamic parameters were evaluated by tracking temperature changes at specific points: specifically at 25°C, 35°C, 45°C, and 55°C. Finally, a mathematical equation was used to calculate the adsorption capacity based on these experimental conditions.

$$q_e = \frac{V(C_0 - C_t)}{m} \qquad (1)$$

where: C_0 represent the initial, while and C_t final concentrations of metal ions (mg/L), respectively.
V stands for the solution's volume (L), while m indicates the adsorbent mass (g).

RESULTS AND DISCUSSION

Characterization of Fe_3O_4/CaO/PDA composite

Figure 1 presents the XRD spectra of Fe_3O_4, Fe_3O_4/CaO, and Fe_3O_4/CaO/PDA. The distinctive peaks of Fe_3O_4 are seen at angles 30.4°, 35.47°, 43.35°, 53.71°, 57.27°, and 62.63°, which are

associated with the crystal planes [220], [311], [400], [422], [511], and [440] in that order as confirmed by JCPDS card No. 19–0629. Fe_3O_4/CaO composite peaks exhibit a reduction in intensity, with some overlap observed between the Fe_3O_4 peak and the appearance of new peaks originating from CaO. These new peaks, specifically at 32.09°, 36.10°, and 46.54° (JCPDS card No. 48–167), can be attributed to CaO. No discernible difference was observed in the diffraction peak of the Fe_3O_4/CaO/PDA composite compared to that of the Fe_3O_4/CaO composite. However, the peak intensity of the Fe_3O_4/CaO/PDA composite was lower than that of the Fe_3O_4/CaO composite. It suggests that PDA lacks a definite form or structure (Shi et al., 2021).

An adsorbent's ability to adsorb is heavily dependent on its surface area. Table 1 provides the measurements of surface areas for CaO, Fe_3O_4/CaO, and Fe_3O_4/CaO/PDA composites. As per Buasri et al. (2013), the derived surface area (86.554 m^2/g) surpasses that of CaO obtained from cookle shell (59.87 m^2/g) and scallop shell (74.96 m^2/g). Fe_3O_4/CaO/PDA composites demonstrated a relatively diminished surface area in comparison to Fe_3O_4/CaO, implying the integration of both Fe_3O_4 and PDA elements within the composite structure. It has been observed that Fe_3O_4 tends to occupy the pores within CaO. A similar phenomenon was also reported in previous research where inclusion of Fe_3O_4/PDA in the Fe_3O_4/PDA/HKUST-1 composite led to a reduction in surface area (Zhou et al., 2023). These observations suggest that incorporation of both Fe_3O_4 and PDA resulted in an expansion in pore diameter when using Barrett-Joyner-Halenda (BJH) adsorption methodology; however, there was a decrease in pore volume. These pores are categorized as mesopores with diameters ranging from 2 to 50 Å (Duan et al., 2020).

Figure 2 illustrates the morphological of CaO, Fe_3O_4/CaO, and Fe_3O_4/CaO/PDA composites. The surface of CaO exhibited an uneven structure. However, notable changes were seen upon introducing Fe_3O_4 and subsequent coating with PDA. Specifically, the surface became rougher, displaying a plate-like morphology, and the emergence of white PDA particles on the surface was evident. The outcomes corroborate the depiction in Figure 3, demonstrating a heterogeneous elemental
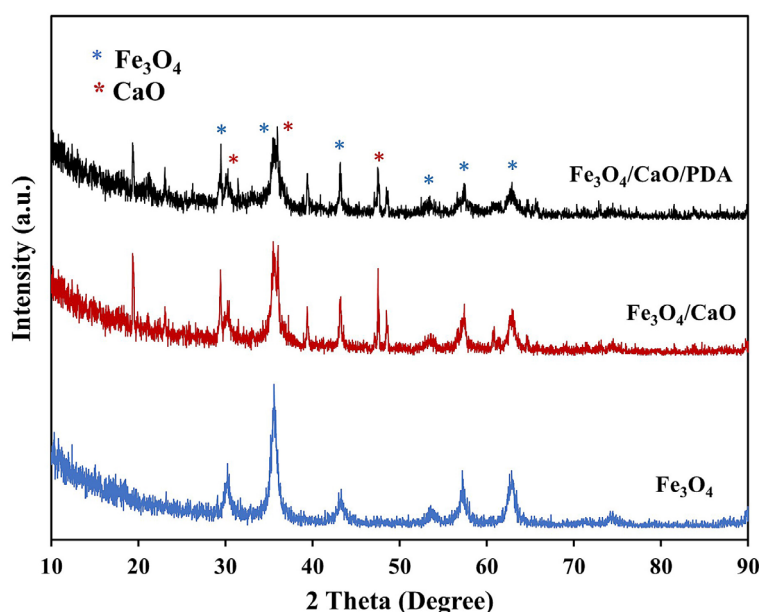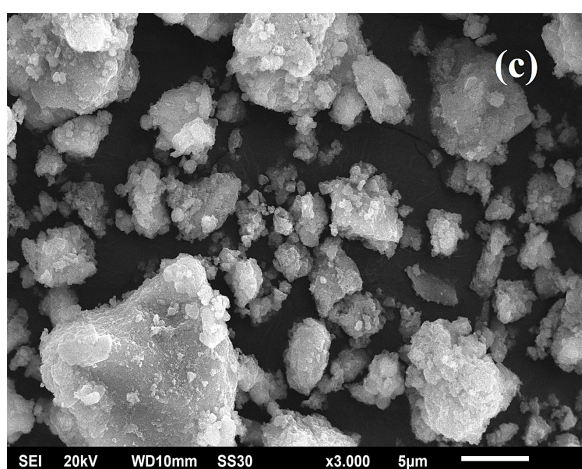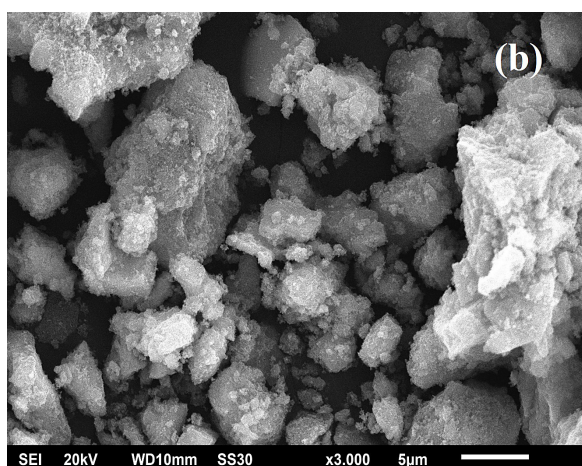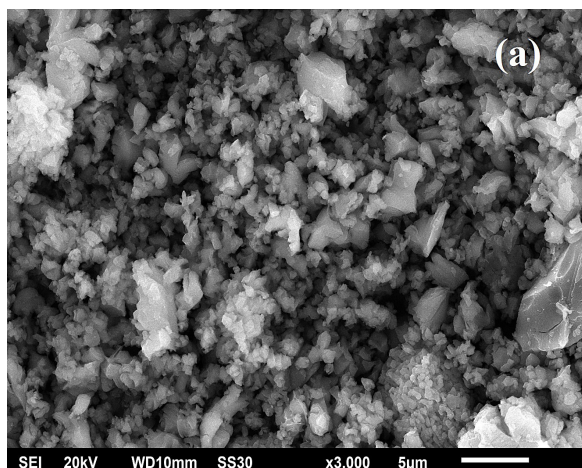

Figure 1. XRD spectra of Fe_3O_4, Fe_3O_4/CaO and Fe_3O_4/CaO/PDA composites

Table 1. The result of surface area measurement of CaO, Fe_3O_4/CaO and Fe_3O_4/CaO/PDA composites

Adsorbent	BET surface area (m^2/g)	Pore volume (cm^3/g)	Pore diameter (Å)
CaO	86.554	0.171	15.14
Fe_3O_4/CaO	74.840	0.161	16.89
Fe_3O_4/CaO/PDA	64.302	0.113	20.41

dispersion across the surface of the Fe_3O_4/CaO/PDA composite. A significant presence of Fe (represented by blue color) implies that Fe_3O_4 not only fills up the pores of CaO but also adheres to its surface. The results from the EDS analysis indicated that the composition of CaO was made up of 68.06% Ca and 31.94% O. The successful synthesis of the Fe_3O_4/CaO/PDA composite is corroborated by the detection of Ca, O, Fe, C, and N elements as demonstrated in Table 2.

Figure 4 illustrates the correlation between magnetization and the magnetic field. The Fe_3O_4/CaO composite demonstrated superior magnetic properties in comparison to the Fe_3O_4/CaO/PDA composite, as indicated by their respective values of 66.28 emu/g and 51.47 emu/g. The reduction in magnetic properties can be ascribed to the non-magnetic PDA coating. As per Shi et al. (2021) findings, PDA/Fe_3O_4 exhibits a saturation magnetization of 37 emu/g, which is higher than that of MnO_2/PDA/Fe_3O_4. The use of these magnetic characteristics provides numerous advantages in terms of efficiency and cost-effectiveness due to the capability for straightforward separation of the adsorbent from the solution using an external magnet, thereby facilitating rapid separation (Hariani et al., 2021).

Batch adsorption of Fe(III) and Mn(II) ions

The pH level exerts a pivotal influence on the adsorption process. This investigation scrutinized the impact of pH, spanning from 1.5 to 5, on the adsorption of Fe(III) and Mn(II) ions, which were employed at concentrations of 100 mg/L and 50 mg/L. The dosage of the composite was fixed at 0.1 g/L, while the stirring speed was kept constant at 150 revolutions per minute. The correlation between initial pH and intrinsic structural attributes of both the adsorbent substance and metal ions has been previously elucidated by Shi et al. (2021).

As illustrated in Figure 5(a), there is a direct correlation between pH level and the amount of metal ions adsorbed. At lower pH values, competition arises between positively charged metal ions and H+ ions for interaction with PDA, which contains O and OH groups (Mansoor & Abbasitabar, 2020; Yang et al., 2021). The optimal pH to achieve maximum adsorption capacity was found to be at a value of 3 for Fe(III) ions and at a value of 4 for Mn(II) ions. Beyond these optimal points, any further increase in pH does not enhance adsorption capacity due to formation of $Fe(OH)_3$ and $Mn(OH)_2$.

This behavior mirrors trends observed in other studies such as that conducted by Brishti et al. (2023), where activated carbon derived from Bombax ceiba fruit shell was used for adsorption of Fe(III) ions with peak efficiency reached at a pH value of around 3.5 before plateauing until about
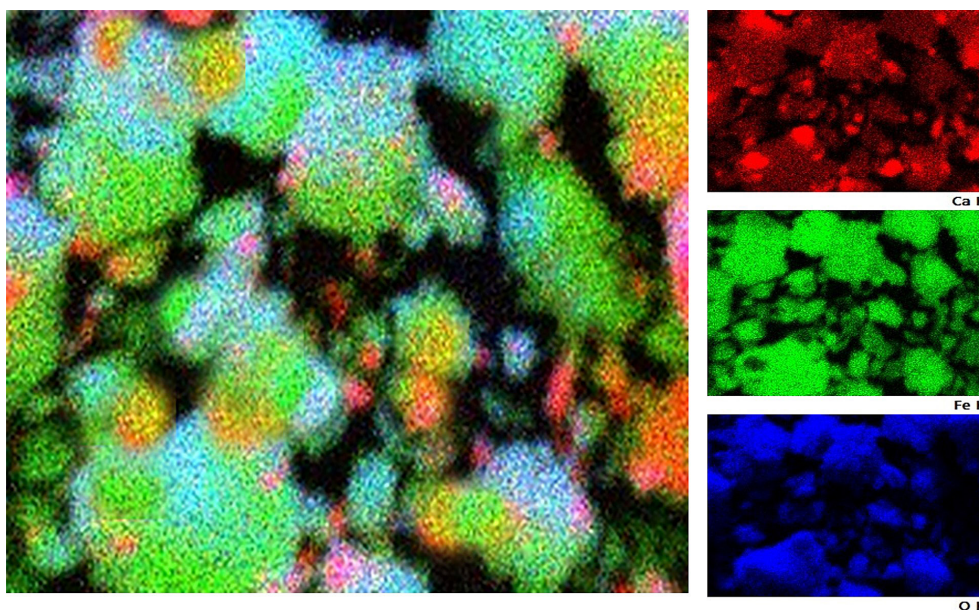

Figure 2. Morphology of (a) CaO, (b) Fe_3O_4/CaO, and (c) Fe_3O_4/CaO/PDA composites

Figure 3. SEM mapping of Fe_3O_4/CaO/PDA composite

Table 2. Elemental composition of CaO, Fe_3O_4/CaO, and Fe_3O_4/CaO/PDA composites from EDS analysis

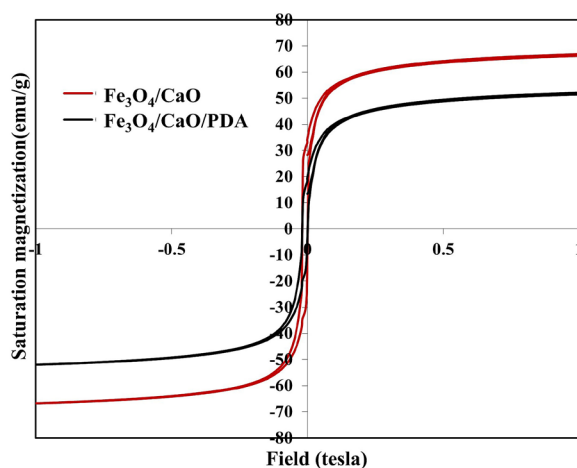| Content, %	CaO	Fe_3O_4/CaO	Fe_3O_4/CaO/PDA
Ca	68.06	26.27	15.32
O	31.94	41.69	34.10
Fe	-	32.04	19.07
C	-	-	29.23
N	-	-	2.28

Figure 4. Hysteresis loops of Fe_3O_4/CaO and Fe_3O_4/CaO/PDA composites

pH value of approximately 5.5. Similarly, another study involving Mn ion absorption using activated carbon derived from banana peel showed optimal performance occurring at a similar point – specifically when reaching a slightly higher pH value around about 4 (Khairiah et al., 2021).

The contact time was optimized over a range of 5 to 60 minutes. The concentration of Fe(III) ions was set at 100 mg/L, and Mn(II) ions were kept at 50 mg/L. A composite dosage of 0.1 g/L was utilized, and the pH of the solution was adjusted to 3 for Fe(III) ions and to 4 for Mn(II) ions. The agitation speed was maintained at 150 rpm. As shown in Figure 5(b), there is an initial rapid uptake of metal ions, which subsequently slows down as it approaches equilibrium–this observation is consistent with prior research by El Shahawy et al. (2022) and Brishti et al. (2023). At a contact time of just five minutes, the adsorption capacity for Fe(III) ions reached 51.23 mg/g, whereas it measured at 17.67 mg/g for Mn(II) ions. After a full hour (60 minutes), these capacities increased to 88.56 mg/g for Fe(III) ions and to 37.93 mg/g for Mn(II) ions respectively.

Figure 5(c) presents data that indicates a direct relationship between the rate of adsorption and the initial concentration of metal ions. The study conducted this adsorption process across a concentration range of 100–450 mg/L.

The upward trend can be ascribed to remaining pores or active sites on the adsorbent material that maintain their capability to attach to metal ions. However, once these sites reach saturation, they lose their ability to accommodate additional metal ions (Brishti et al., 2023). No noticeable increase in metal ion adsorption was observed for both Fe(III) and Mn(II) ions at an initial concentration of 450 mg/L.
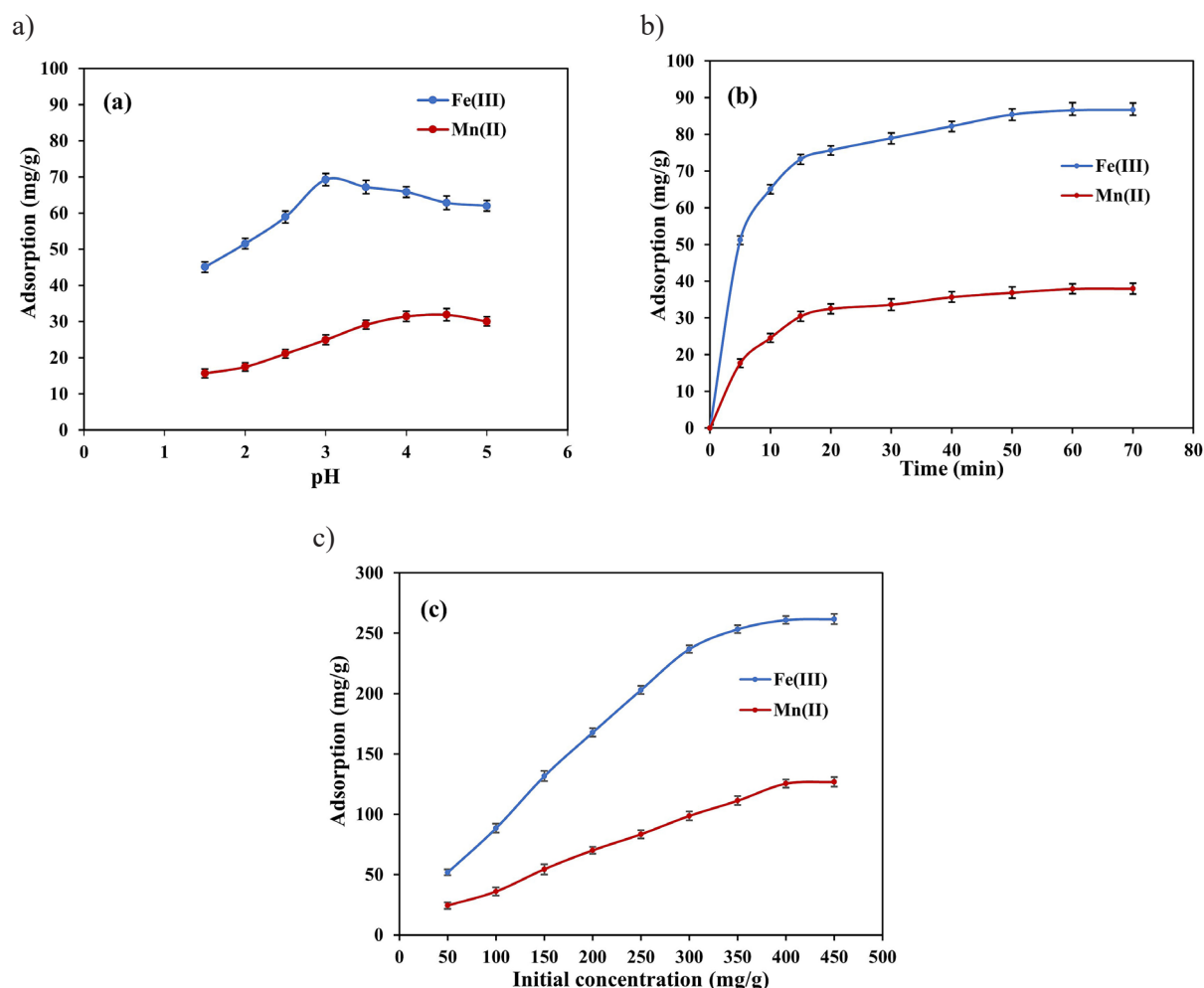
FTIR spectra of composite pre- and post-adsorption

Figure 6 presents the spectra of the $Fe_3O_4/CaO/PDA$ composite before and after the adsorption procedure. The spectra reveal a broad peak within the 3200–3400 cm^{-1} range, indicative of O–H and N–H stretching vibrations. A band at 1600 cm^{-1} corresponds to N–H bond movements, encompassing both stretching and bending modes (Touqeer et al., 2020). A peak located at 1290 cm^{-1} suggests the existence of a C–O bond.

All three spectra feature an Fe–O band located at 569 cm^{-1}, indicative of Fe_3O_4's presence. According to Legodi et al. (2001), a peak appearing between 1400–1500 cm^{-1} together with another near 873 cm^{-1} implies swift transformation from hydroxide into carbonate. This specific peak can be seen in the spectra for the $Fe_3O_4/CaO/PDA$ composite following the ions adsorption. As delineated by Kasirajan et al. (2022), any shift in wavenumber below 10 cm^{-1}, accompanied by alterations in peak intensity, is indicative of the formation of metal ion bonds with the adsorbent substrate.

Adsorption kinetics and isotherm

The importance of kinetics in evaluating the effectiveness of adsorption is underscored in the work of Moghadam et al. (2013). Within the realm of adsorption kinetics, two models are predominantly used: the pseudo-first-order and pseudo-second-order models. These can be signified mathematically through these equations.

a)

b)

c)

Figure 5. The impact of variable on the adsorption including
(a) pH, (b) Contact time, and (c) Initial concentration.
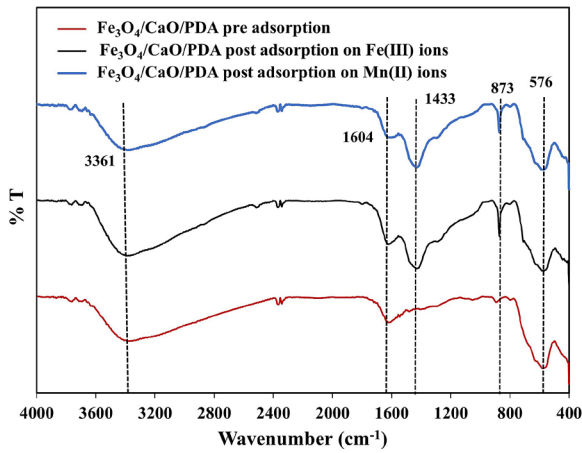
Figure 6. The comparison of FTIR spectra of the Fe$_3$O$_4$/CaO/PDA composite pre- and post-adsorption.

$$\ln(q_e - q_t) = \ln q_e - k_1 t \qquad (2)$$

$$\frac{t}{q_t} = \frac{1}{k_2 q_e^2} + \frac{t}{q_e} \qquad (3)$$

The variables q_t (mg/g) are indicative of the adsorption potential at a given time (t), while q_e (mg/g) denotes the potential when equilibrium is reached. The parameters k_1 (min^{-1}) correspond to the equilibrium states of pseudo-first-order, whereas k_2 (g/mg.min) pseudo-second-order reactions. The pseudo-second-order model exhibits a superior regression coefficient (R^2) when compared to the first-order model, suggesting that it provides a more accurate representation of the adsorption dynamics of Fe(III) and Mn(II) ions onto the Fe$_3$O$_4$/CaO/PDA composite.

The pseudo-first-order process characterizes a reversible reaction that creates an equilibrium between the solid and liquid phases. In contrast, the pseudo-second-order process implies chemical adsorption takes place (Yang et al., 2021). The adsorption capacity determined by the pseudo-second-order kinetic model shows greater concordance with experimental results compared to its pseudo-first-order counterpart (Table 3). Parallel results were found in a separate study, which established that the adsorption of melamine on Fe(III) and Mn(II) ions adheres to a pseudo-second-order kinetic model (Peng et al., 2020).

Adsorption isotherms shed light on the connection between the concentration of adsorbent in the solid phase and its presence in the liquid phase under balanced conditions (Keshavarza et al., 2020). The adsorption isotherms for Fe(III) and Mn(II) ions were studied using two distinct frameworks, namely, the Langmuir isotherm and Freundlich isotherm. The linear formulations for both Langmuir and Freundlich isotherms can be articulated as follows.

$$\frac{C_e}{q_e} = \frac{C_e}{q_m} + \frac{1}{K_L q_m} \qquad (4)$$

$$\log q_e = \log K_F + \left(\frac{1}{n}\right) \log C_e \qquad (5)$$

The variable used in equations is as follows. The maximum adsorption capacity represented in q_m (mg/g). K_L (L/mg) is a constant on the Langmuir isotherm, while K_F is the Freundlich constant (mg/g)(mg/L). The intensity and surface heterogeneity at different concentrations is denoted by $1/n$ (Wang et al., 2019).

Table 4 presents the adsorption parameters of Fe(III) and Mn(II) ions using the Fe$_3$O$_4$/CaO/PDA composite. The R^2 for the Langmuir isotherm is closer to 1 than the Freundlich isotherm. This observation suggests that the adsorption process of Fe(III) and Mn(II) ions onto this composite occurs predominantly as a monolayer, consistent with the principles of Langmuir adsorption (Dai et al., 2012)

Table 3. The kinetics parameters for the adsorption of Fe(III) and Mn(II) ions

Adsorption kinetics	Fe(III)	Mn(II)
Pseudo-first-order		
R^2	0.9692	0.9731
k_1 (min^{-1})	0.0969	0.973
$q_{e\ (calc)}$ (mg/g)	39.18	23.21
Pseudo-second-order		
R^2	0.9971	0.9948
k_2 (g/mg·min)	0.0031	0.0238
$q_{e\ (calc)}$ (mg/g)	90.91	42.07
$e_{(eksp)}$ (mg/g)	85.41	36.92

Table 4. The parameter of isotherm in the adsorption of Fe(III) and Mn(II) ions

Isotherm adsorption	Fe(III)	Mn(II)
Langmuir		
R^2	0.9962	0.9951
K_L (L/mg)	0.361	0.085
q_m (mg/g)	322.58	208.33
Freundlich		
R^2	0.9696	0.9931
K_F (g/mg.min)	27.88	4.78
n	2.006	1.549

Table 5 provides a comparative evaluation of the capacity of adsorption of different adsorbents for Fe(III) and Mn(II) ions. The adsorption capacity exhibited in this research exceeds those reported in prior studies.

The thermodynamics of the adsorption

The influence of temperature on adsorption capacity is a fundamental aspect in the study of adsorption thermodynamics. To elucidate this, a sequence of experiments was conducted at distinct temperatures, specifically 25°C, 35°C, 45°C, and 55°C. The examination incorporated key thermodynamic parameters such as Gibbs free energy ($\Delta G°$), enthalpy change ($\Delta H°$), and entropy change ($\Delta S°$). The computation of these parameters is achieved through specific thermodynamic equations.

$$ln(\frac{q_e}{C_e}) = \frac{\Delta S°}{R} - \frac{\Delta H°}{RT} \tag{6}$$

In the equation, R stands for the universal gas constant, which has a value of 8.314 J/mol K. T denotes the absolute temperature expressed in Kelvin (K). To derive the values of $\Delta H°$ and $\Delta S°$, a plot is created with $ln(q_e/C_e)$ on the y-axis and 1/T on the x-axis. The slope and intercept of this plot correspond to $\Delta H°$ and $\Delta S°$ respectively. The $\Delta G°$ can then be calculated using an appropriate formula:

$$\Delta G° = \Delta H° - T\Delta S° \tag{7}$$

The data presented in Table 6 indicates that the binding of Fe(III) and Mn(II) ions to the Fe_3O_4/CaO/PDA composite is an exothermic process, as evidenced by the positive $\Delta H°$ values. In contrast, the negative $\Delta S°$ values imply that these adsorption processes are not only spontaneous but also irreversible when it comes to metal adsorption. The appearance of negative $\Delta G°$ values at various temperatures indicates a tendency towards spontaneity in the adsorption process. Moreover, as temperature increases, there is a corresponding rise in $\Delta G°$ value, suggesting an increased propensity for adsorption with higher temperatures.

Table 5. A comparative analysis of the capacity of Fe(III) and Mn(II) ions to be absorbed into various adsorbents

Ions	Adsorbent	pH	Initaial concentration (mg/L)	Time (min)	Capacity (mg/g)	Reference
Fe(III)	Chitosan	3	6	60	90.09	Ngah et al., 2005
	Hazelnut hull	3	20	70	13.59	Sheibani et al., 2012
	Zeolite NaY	5	120	30	57.80	Kulawong and Kulawong, 2018
	Brown bentonite	-	200	120	16.65	Bakalar et al., 2020
	Activated carbon from Bombax ceiba fruit shell	3.5	75	25	37.16	Brishti et al., 2023
	Fe_3O_4/CaO/PDA	3	400	60	322.58	In this study
Mn(II)	Chitosan/poly ethylene glycol blend membrane	6	10	80	21.7	Reiad et al., 2012
	Natural zeolite	6	25–250	240	7.68	Ates, 2014
	Carbon impregnated CTAB	7	50	420	43	Anbia et al., 2016
	Banana peels-activated carbon	4	1.351	30	-	Khairiah et al., 2021
	Blast furnace slag	5.2	30	50	59.88	Chouchane et al., 2023
	Fe_3O_4/CaO/PDA	5	400	60	208.33	In this study

Table 6. Thermodynamic parameters for the adsorption of Fe(III) and Mn(II) ions

Ions	Parameters (kJ/mol)	Temperature (°C)			
		25	35	45	55
Fe(III)	ΔG°	-24.956	-25.399	-25.842	-26.284
	ΔH°	-11.754			
	ΔS°	0.044			
Mn(II)	ΔG°	-19.498	-19.814	-20.130	-20.446
	ΔH°	-10.075			
	ΔS°	0.032			

CONCLUSION

CaO was effectively derived from the shells of green mussels and used as a precursor for the manufacture of composites consisting of Fe_3O_4, CaO, and PDA. The composite of Fe_3O_4/CaO/PDA shown a notable adsorption capacity for Fe(III) and Mn(II) ions, specifically measuring 322.58 mg/g and 208.33 mg/g. A further advantage of Fe_3O_4/CaO/PDA composite is its simple separation from the solution, which can be accomplished in a short amount of time using an external magnet, the separation procedure is more cost-effective. The results indicate that the Fe_3O_4/CaO/PDA composite has promising remediation potential for acid mine runoff. AMD is characterized by a heightened presence of heavy metal ions, hence requiring the adoption of a suitable resolution to address this issue.

Acknowledgment

REFERENCES

1. Aguila-Almanza, E., Hernandez-Cocoletzi, H., Rubio-Rosas, E., Calleja-Gonzales, M., Lim, H.R., Khoo, K.S., Singh, V., Maldonado-Montiel, J.C., Show, P.L. 2022. Recuperation and characterization of calcium carbonate from residual oyster and clamshells and their incorporation into a residential finish. Chemosphere, 288, 1–9.

2. Ambiado, K., Bustos, C., Schwarz, A., Bórquez, R. 2017. Membrane technology applied to acid mine drainage from copper mining. Water Science & Technology, 75, 705–715.

3. Anbia, M., Amirmahmoodi, S. 2016. Removal of Hg(II) and Mn(II) from aqueous solution using nanoporous carbon impregnated with surfactants. Arabian Journal of Chemistry, 9(1), S319–S325.

4. Ates, A. 2014. Role of modification of natural zeolite in removal of manganese from aqueous solutions. Powder Technology, 264, 86–95.

5. Ayodeji, A.A., Blessing, I.E., Sunday, F.O. 2018. Data on calcium oxide and cow bone catalysts used for soybean biodiesel production. Data in Brief, 18, 512–517.

6. Bakalár, T., Kaˇnuchová, M., Girová, A., Pavolová, H., Hromada, R., Hajduová, Z. 2020. Characterization of Fe(III) adsorption onto zeolite and bentonite. International Journal of Environmental Research and Public Health, 17, 1–13.

7. Brishti, R.S., Kundu, R., Habib, Md. A., Ara, M.H. 2023. Adsorption of iron(III) from aqueous solution onto activated carbon of a natural source: Bombax ceiba fruit shell. Results in Chemistry, 5, 1–6.

8. Buasri, A., Chaiyut, N., Laryuenyong, V., Worawanitchaphng, P., Trongyong, S. 2013. Calcium oxide derived from waste shells of Mussel, Cockle, and Scallop as the heterogeneous catalyst for biodiesel production. The Scientific World Journal, 2013, 1–8.

9. Chen, D., Wang, G., Chen, C., Feng, Z., Jiang, Y., Yu, H., Li, M., Chao, Y., Tang, Y., Wang, S., Qiu, R. 2023. Membrane technology applied to acid mine drainage from copper mining. Journal of Hazardous Materials, 454, 1–18.

10. Chouchane, T., Boukari, A., Khireddine, O., Chibani, S., Chouchane, S. 2023. Equilibrium, kinetics, and thermodynamics of batch adsorption of Mn(II) ions on blast furnace slag (BFS) and kaolin (KGA). Journal of Engineering and Applied Science, 70(58), 1–20.

11. Dai, J. Ren, F., Tao, C.Y. 2012. Adsorption behavior of Fe(II) and Fe(III) ions on thiourea cross-linked chitosan with Fe(III) as template. Molecules, 17, 4388–4399.

12. Deng, D., Weidhaas, J.L., Lin, L.S. 2016. Kinetics and microbial ecology of batch sulfidogenic

bioreactors for co-treatment of municipal wastewater and acid mine drainage. Journal of Hazardous Materials, 305, 200–208.

13. Duan, Z., Zhang, W., Lu, M., Shao, Z., Huang, W., Li, J., Li, Y., Mo, J., Li, Y., Chen, C. 2020. Magnetic Fe3O4/activated carbon for combined adsorption and Fenton oxidation of 4-chlorophenol. Carbon, 167, 351–363.

14. El Shahawy, A., Mubarak, M.F., El Shafied, M., Abdulla, H.M. 2022. Fe(III) and Cr(VI) ions' removal using AgNPs/GO/chitosan nanocomposite as an adsorbent for wastewater treatment. RSC Advances, 12, 17065–17084.

15. Favere, V.T., Laus, R., Laranjeira, M.C.M., Martins, A.O., Pedrosa, R.C. 2004. Use of chitosan microspheres as remedial material for acidity and iron (III) contents of coal mining wastewaters. Environmental Technology, 25(8), 861–866.

16. Hamestera, M.R.R., Balzera, P.S., Becker, D. 2012. Characterization of calcium carbonate obtained from Oyster and Mussel shells and incorporation in polypropylene. Materials Research, 15(2), 204–208.

17. Hariani, P.L, Said, M., Rachmat, A., Sari, S.P. 2021. Hydroxyapatite-PEG/Fe$_3$O$_4$ composite for adsorption of phenol from aqueous solution. Polish Journal of Environmental Studies, 30(2), 1621–1629.

18. Hossain, M., Muntaha, N., Goni, L.K.M.O., Jamal, M.S., Gafur, M.A., Islam, D., Fakhruddin, A.N.M. 2021. Triglyceride conversion of waste frying oil up to 98.46% using low concentration K+/CaO Catalysts Derived from Eggshells. ACS Omega, 2021, 6(51), 35679–35691.

19. Hossain, Md.S., Jahan, S.A., Ahmed, S. 2023. Crystallographic characterization of bio-waste material originated CaCO3, green-synthesized CaO and Ca(OH)2. Results in Chemistry, 5, 1–8.

20. Kasirajan, R., Bekele, A., Girma, E. 2022. Adsorption of lead (Pb-II) using CaO-NPs synthesized by solgel process from hen eggshell: Response surface methodology for modeling, optimization and kinetic studies. South African Journal of Chemical Engineering, 40, 209–229.

21. Khairiah, K., Frida, E., Sebayang, K., Sinuhaji, P., Humaidi, S. 2021. Data on characterization, model, and adsorption rate of banana peel activated carbon (Musa Acuminata) for adsorbents of various heavy metals (Mn, Pb, Zn, Fe). Data in Brief, 39, 1–9.

22. Keshavarza, M., Foroutanb, R., Paparic, F., Bulgariud, L., Esmaeili, H. 2020. Synthesis of CaO/Fe$_2$O$_3$ nanocomposite as an efficient nanoadsorbent for the treatment of wastewater containing Cr (III). Separation Science and Technology, 56(8), 1328–1341.

23. Kobielska, P.A., Howarth, A.J., Farha, O.K., Nayak, S. 2018. Metal–organic frameworks for heavy metal removal from water. Coordination Chemistry Reviews, 358, 92–107.

24. Kulawong S., Kulawong, J. 2018. Adsorpstion efficiency of Fe(III) from solution by Zeolite Y synthesized from rice husk. Naresuan University Journal: Science and Technology, 26, 144–156.

25. Legodi, M.A., De Waal, D., Potgieter, J.H., Potgieter, S.S. 2001. Rapid determination of CaCO$_3$ in mixtures utilizing FT–IR spectroscopy. Minerals Engineering, 14(9), 1107–1111

26. Li, J., Han, W., Liu. H., Su, M., Chen, D., Song, G. 2023. Simultaneous removal of Cs(I) and U(VI) by a novel magnetic AMP/PDA/Fe$_3$O$_4$ composite. Journal of Cleaner Production, 409, 1–11.

27. Masindi, V., Gitari, M.W., Tutu, H., De Beer, M., 2015. Passive remediation of acid mine drainage using cryptocrystalline magnesite: a batch experimental and geochemical modelling approach. Water SA, 41(5), 677–682.

28. Mansoor, S.J., Abbasitabar, F. 2020. Adsorption behavior of Fe(II) and Fe(III) ions on polyaniline coated sawdust: batch and fixed–bed studies. Acta Chimica Slovenica, 67, 36–46.

29. Menzel, K., Barros, L., Garcia, A., Ruby-Figueroa, Estay, H. 2021. Metal sulfide precipitation coupled with membrane filtration process for recovering copper from acid mine drainage. Separation and Purification Technology, 270, 1–13.

30. Miri, Z., Elhami, S., Zare-Shahabadi, V., Jahromi, H.J. 2021. Fe$_3$O$_4$/PDA/PANI core–shell nanocomposites as a new adsorbent for simultaneous preconcentration of Tartrazine and Sunset Yellow by ultrasonic-assisted dispersive micro solid-phase extraction. Spectrochimica Acta Part A: Molecular and Biomolecular Spectroscopy, 262, 1–9.

31. Moghadam, M.R., Nasirizadeh, N., Dashti, Z., Babanezhad, E. 2013. Removal of Fe(II) from aqueous solution using pomegranate peel carbon: equilibrium and kinetic studies. International Journal of Industrial Chemistry, 4(19), 1–6.

32. Mohamed, M., Yusup, S., Bustam, M.A. 2016. Synthesis of CaO-based Sorbent from Biomass for CO$_2$ Capture in Series of Calcination-carbonation Cycle. Procedia Engineering, 148,78–85.

33. Mokgehle, T.M., Tavengwa, N.T. 2021. Recent developments in materials used for the removal of metal ions from acid mine drainage. Applied Water Science, 11(42), 1–11.

34. Mostofa, S., Jahan, S.A., Saha, B., Sharmin, N., Ahmed, S. 2022. Kinetic and thermodynamic investigation on adsorption of lead onto apatite extracted from mixed fish bone. Environmental Nanotechnology, Monitoring & Management, 18, 1–11.

35. Ngah, W.S.W., Ab Ghani, S., Kamari, A. 2005. Adsorption behaviour of Fe(II) and Fe(III) ions in aqueous solution on chitosan and cross-linked chitosan beads. Bioresource Technology, 96, 443–450.

36. Nunez-Gomez, D., Rodrigues, C., Lapolli, F.R., Lobo-Recio, M.A. 2019. Adsorption of heavy metals from coal acid mine drainage by shrimp shell waste: Isotherm and continuous-flow studies. Journal of Environmental Chemical Engineering, 7, 1–10.

37. Peng, H., Guo, J., Wang, B. 2020. Adsorption behavior of Fe(III) in aqueous solution on melamine. Water Science & Technology, 82(9), 1848–1857.

38. Purwaningrum, W., Hasanudin, H., Rachmat, A., Riyanti, F., Hariani, P.L. 2022. Modification of calcium oxide from Green Mussel Shell with iron oxide as a potential adsorbent for the removal of iron and manganese ions from acid mine drainage. Journal of Ecological Engineering, 23(11), 188–201.

39. Reiad, N.E., Salam, O.E.A., Abadir, E.F., Harraz, F.A. 2012. Adsorptive removal of iron and manganese ions from aqueous solutions with microporous chitosan/polyethylene glycol blend membrane. Journal of Environmental Sciences, 24(8), 1425–1432.

40. Ren, J., Zheng, L., Su, Y., Meng, P., Zhou, Q., Zeng, H., Zhang, T., Yu, H. 2022. Competitive adsorption of Cd(II), Pb(II) and Cu(II) ions from acid mine drainage with zero-valent iron/phosphoric titanium dioxide: XPS qualitative analyses and DFT quantitative calculations. Chemical Engineering Journal, 445, 1–14.

41. Sheibani, A., Shishehbor, M.R., Alaei, H. 2012. Removal of Fe(III) ions from aqueous solution by hazelnut hull as an adsorbent. International Journal of Industrial Chemistry, 3(4), 1–4.

42. Shi, S., Xu, C., Dong, Q., Wang, Y., Zhu, S., Zhang, X., Chow, Y.T., Wang, X., Zhu, L., Zhang, G., Xu, D. 2021. High saturation magnetization MnO_2/PDA/Fe_3O_4 fibers for efficient Pb(II) adsorption and rapid magnetic separation. Applied Surface Science, 541, 1–11.

43. Stylianou, M., Montel, E., Zissimos, A., Christoforou, I., Dermentzis, K., Agapiou, A. 2022. Removal of toxic metals and anions from acid mine drainage (AMD) by electrocoagulation: The case of North Mathiatis open cast mine. Sustainable Chemistry and Pharmacy, 29, 1–13.

44. Thakur, S., Singh, S., Pal, B. 2021. Superior adsorption removal of dye and high catalytic activity for transesterification reaction displayed by crystalline CaO nanocubes extracted from mollusc shells. Fuel Processing Technology, 213, 1–9.

45. Touqeer, T., Mumtaz, M.W., Mukhtar, H., Irfan, A., Akram, S., Shabbir, A., Rashid, U., Nehdi, I.A., Choong, TSY 2020. Fe_3O_4-PDA-Lipase as Surface Functionalized Nano Biocatalyst for the Production of Biodiesel Using Waste Cooking Oil as Feedstock: Characterization and Process Optimization. Energies, 13(17), 1–19.

46. Valente, T., Grande, J.A., de la Torre, M.L., Gomes, P., Santisteban, M., Borrego, J., Braga, M.A.S. 2015. Mineralogy and geochemistry of a clogged mining reservoir affected by historical acid mine drainage in an abandoned mining area. Journal of Geochemical Exploration, 157, 66–76.

47. Wang, T., Chen, P., Li, M., Luo, X., Liu, L., Zeng, G., Jiang, J., Huang, K., Xu, X., Li, S., Jiang, H. 2019. Synthesis of $La_2(C_2O_4)_3$ nanoprisms decorated with Fe_3O_4/m(ZrO_2-CeO_2) nanospheres and their application for effective fluoride removal. Journal of Chemical Technology and Biotechnology, 94(11), 3650–3660.

48. Yang, H., Ding, H., Zhang, X., Luo, X., Zhang, Y. 2019. Immobilization of dopamine on Aspergillus niger microspheres (AM/PDA) and its effect on the U(VI) adsorption capacity in aqueous solutions. Colloids and Surfaces A: Physicochemical and Engineering Aspects, 583, 1–10.

49. Xu, Q., Yue, Z., deng, R., Wang, X., Chuai, X., Zhang, K., Wang, J. 2023. Process and mechanism of recovering layered double hydroxides (LDHs) from acid mine drainage (AMD) and synergetic removal of manganese. Journal of Environmental Chemical Engineering, 11(5), 1–12.

50. Yang, M., Lu, C., Quan, X., Cao, D. 2021. Mechanism of acid mine drainage remediation with steel slag: a review. ACS Omega, 6(45), 30205–30213.

51. Zhou, G., Wang, Q., Song, R., Li, S., Yang, S., Zhang, Q. 2023. Synthesis of core-double-shell structured Fe_3O_4/PDA/HKUST-1: Characterization analysis and adsorption performance on cationic MB dyes. Journal of Physics and Chemistry of Solids, 172, 1–11.